Crack Shear in Concrete: Crack Band Microplane Model

By Zdeněk P. Bažant,[1] F. ASCE and Pietro G. Gambarova,[2] M. ASCE

Abstract: The crack band model is applied to the problem of crack shear in concrete. The constitutive law for concrete within the crack band is provided by the microplane model, in which the microstrains on weak planes of various orientations (the microplanes) are assumed to conform to the same macroscopic strain tensor, and the microstresses from all the microplanes are superimposed. Due to the neglect of shear stiffness on individual microplanes, the material behavior is completely characterized by the relation between the normal stress and strain for each microplane. To simulate crack shear, the law for unloading contribution on the microplanes after previous tensile strain-softening is important, since the shear stresses resisting crack shear, as well as the normal confining stresses and crack dilatancy, result from compression along lines inclined with regard to the crack plane. A satisfactory agreement with the existing results from shearing tests of cracked concrete blocks (i.e., aggregate interlock tests) is achieved. Since the same type of model was previously shown capable of modeling strain-softening in direct tensile tests, fracture of notched specimens, and deflections of cracked reinforced beams, the present model appears to have a general applicability. It can be applied to the shearing of cracks only partially formed (a system of distinct discontinuous cracks still in the strain softening stage), to cracks that are being produced simultaneously with shearing, to crack shear when the direction of shearing within the crack plane rotates, and to shearing of concrete intersected by cracks of various directions. Thus, the model appears suitable for general finite element programs.

Introduction

In many types of failure, the carrying capacity of concrete structures strongly depends on the transmission of shear stresses across cracks. The capability of concrete to transmit shear stresses is substantial, due to surface roughness (aggregate interlock mechanism). On the other hand, the shear transmission capability is considerably less than that of intact concrete, and deformations due to shear are much larger. Obviously, an accurate mathematical model for the crack shear is needed for finite element analysis of failures sensitive to crack shear, such as the diagonal shear failure of beams and panels, horizontal shear failure of nuclear containments due to earthquake, cryptodome failure of the top slab in a concrete reactor vessel, punching shear failure of slabs, torsional failure of beams, etc.

Extensive experimental information has been acquired in various shear tests of concrete blocks intersected by distinct, continuous cracks previously formed by tension (14,21,23,24,28,29,36). These test data serve as the basis for development of mathematical models for crack shear, describing the dependence of the shear and normal stresses transmitted

[1]Prof. of Civ. Engrg. and Dir., Center for Concrete and Geomaterials, Northwestern Univ., Evanston, Ill. 60201.

[2]Visiting Scholar, Northwestern Univ., Prof. of Struct. Engrg. on leave from Politecnico di Milano, Italy.

Note.—Discussion open until February 1, 1985. To extend the closing date one month, a written request must be filed with the ASCE Manager of Technical and Professional Publications. The manuscript for this paper was submitted for review and possible publication on October 12, 1983. This paper is part of the *Journal of Structural Engineering*, Vol. 110, No. 9, September, 1984. ©ASCE, ISSN 0733-9445/84/0009-2015/$01.00. Paper No. 19145.

across a crack on the relative slip and opening displacements (7,18,19,32). From fracture studies it is now becoming clear, however, that distinct, continuous cracks represent a rare, idealized situation [Fig. 1(*a*)], and that a more typical practical situation involves shear loading on cracks that are only partially formed, consisting of a band of discontinuous cracks or microcracks [Fig. 1(*b*)].

A more general model, describing the shear of both fully and partially

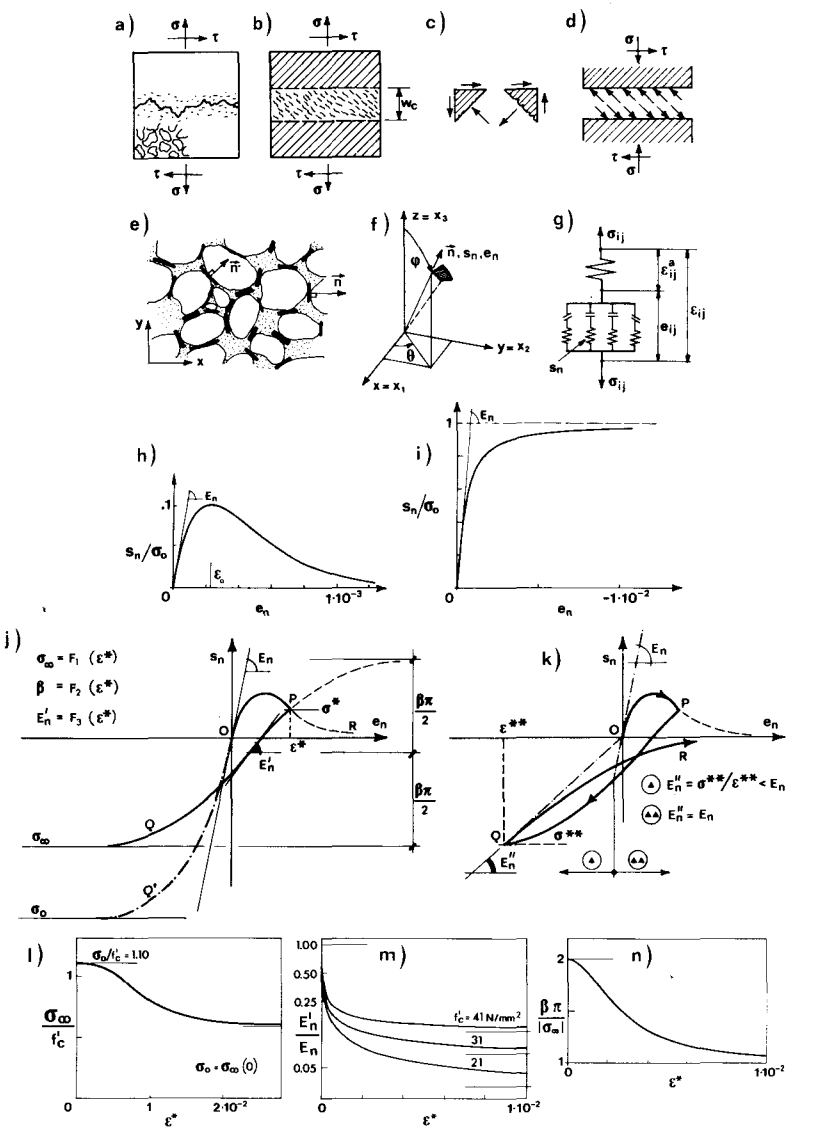

FIG. 1.—(*a–g*) Explanatory Sketches; (*h–k*) Uniaxial Stress-Strain Curves; and (*l–n*) Assumed Elementary Material Properties

formed cracks, is therefore needed. Evidently, such model should describe not only the shear transmission capability of existing cracks, but also the process of formation of the cracks themselves. Development of such a model is chosen as the objective of this study.

Crack Band Theory

It is now generally accepted that fracture in concrete, as well as many other materials, forms by progressive microcracking within a certain relatively large fracture process zone at the fracture front. This process of gradual microcracking may be described by a stress-strain relation that exhibits tensile strain-softening, i.e., a gradual decline of the tensile stress at increasing strain. The existence of tensile strain-softening was clearly confirmed experimentally by Evans and Marathe (17), Petersson (30), and others (20,22,33) (see also Reinhardt and Cornelissen, *Cement and Concrete Research*, Vol. 14, 1984, pp. 263–270). Based on arguments of objectivity and convergence of the mathematical model, as well as analysis of strain-localization instability, it was shown that the width of the crack band at its front should be considered as a fixed material property (3,13). The crack band model has made it possible to achieve good fits of essentially all basic experimental data on the fracture of concrete, both the maximum load data for various types of specimens and the resistance curve (*R*-curve) data, and also the data from direct tensile tests of unnotched specimens (16,37). From the analysis of these test data it also appeared that the width of the crack band front should be taken three times the maximum aggregate size for normal concretes. Furthermore, the strain-softening stress-strain relation used here was further shown to give good results for deflections of cracked reinforced concrete beams, short time as well as long time (12).

In finite element modeling, the crack band is represented by a band of cracked finite elements, having a single-element width at the front. As in the original cracking model of Rashid (31), the cracks are assumed to be continuously distributed, i.e., smeared over the element. The multiaxial constitutive law that includes strain-softening has been originally formulated as a total stress-strain relation, analogous to the deformation theory of plasticity. This formulation is, however, path-independent and can be applied only to situations in which the principal stress directions do not rotate substantially during the fracture formation, i.e., during strain-softening. This limitation can be avoided by a more general approach, called the microplane model, which attempts to describe the progressive formation of microcracks on weak planes of various orientations within the material (9,11).

Microplane Model

Strain-softening violates the basic hypothesis of the theory of plasticity, usually expressed as Drucker's stability postulate. The presence of friction on microcracks and the degradation of elastic stiffness due to progressive microcracking also invalidate Drucker's postulate, as well as the dual Ilyushin's postulate for inelastic potential theory in the strain

space. Thus, the theories that use loading surfaces and inelastic potentials can hardly provide a good model for progressive microcracking. Their use would be further complicated by the fact that the microcracks cause the elastic stiffness to become anisotropic.

For these reasons, it appears preferable to describe the inelastic properties not globally but individually for planes of various orientations within the material. The microscopic deformations on these planes, called the microplanes, must be suitably constrained to the macroscopic deformations. This approach brings about conceptual simplicity in that the tensorial invariance restrictions, which greatly complicate the formulation of the macroscopic inelastic constitutive laws, do not have to be introduced in order to describe the behavior on a plane of specified orientation within the material. The invariance restrictions are satisfied only subsequently, by a suitable combination of planes of various orientations. For example, in the case of isotropy, each orientation must be equally frequent.

The idea of defining the inelastic behavior independently on planes of various orientations within the material [Fig. 1(*e*), and then in some way superimposing the inelastic effects from all the planes, arose in the work of Taylor (35) on plasticity of polycrystalline metals. Batdorf and Budianski (2) developed this idea in their slip theory of metal plasticity, in which the stresses acting on various slip planes are obtained by resolving the macroscopic applied stress, and the plastic strains (slips) from the planes of all directions are then superimposed. A similar superposition of inelastic strains was used in the so-called multilaminate models of Zienkiewicz et al. (38) and Pande et al. (26,27), and in many works on plasticity of polycrystals.

To model the tensile strain-softening of concrete due to microcracking, it is necessary, however, to modify these approaches in that the microstructure is constrained kinematically rather than statically, i.e., the strains on planes of various orientations are the resolved components of the same macroscopic strain, instead of stresses on planes of various orientations being the resolved components of the same macroscopic stress. A model of this type has recently been developed by Bažant and Oh (9) and has been shown to match well the available test data from direct tensile tests. The basic assumptions of this model may be summed up in the following 2 hypotheses:

Hypothesis I.—The normal microstrain, e_n, that governs the progressive development of cracking on a microplane of any orientation is equal to the resolved macroscopic strain tensor, e_{ij}, for the same plane, i.e.,

$$e_n = n_i n_j e_{ij} \quad (1)$$

Here, latin lower case subscripts refer to cartesian coordinates x_i ($i = 1, 2, 3$); n_i are the direction cosines of the unit normal $\vec{n}$ of the microplane; and repeated latin lower case subscripts indicate a summation over 1, 2, 3.

Hypothesis II.—The stress relaxation due to all microcracks normal to $\vec{n}$ is characterized by assuming that the microstress, s_n, on the microplane of any orientation is a function of the normal microstrain, e_n, on the same plane, i.e.,

$$s_n = \frac{2\pi}{3} F(e_n) \quad \ldots\ldots (2)$$

The factor $2\pi/3$ is introduced just for convenience.

Compared to the slip theory of metal plasticity, Hypothesis II differs by dealing with normal rather than shear components, and Hypothesis I by involving strains rather than stresses. There are 3 reasons for Hypothesis I:

1. Using resolved stresses rather than strains on the microplanes would cause computational problems for strain-softening, since two strains correspond to a given stress, but only one stress corresponds to a given strain.
2. The microstrains must be stable when the macrostrains are fixed. It has been experienced numerically that, in the case of strain-softening, the model becomes unstable if resolved stresses rather than strains are used in Hypothesis I.
3. The use of resolved strains, rather than stresses, seems to describe better what is happening in the microstructure of a brittle aggregate material. The use of resolved stresses is reasonable for polycrystals in which local slips scatter widely, while the stress is more or less uniformly distributed throughout the microstructure. By contrast, in a brittle aggregate material consisting of hard inclusions embedded in a weak matrix, the stresses are far from uniform, having sharp extremes at the locations where the surfaces of aggregate pieces are nearest. The deformation of the thin contact layer of matrix between two aggregate pieces, which yields the major contribution to inelastic strain, is determined chiefly by the relative displacements of the centroids of the two aggregate pieces, which roughly correspond to the macroscopic strain. The microplanes may be imagined to represent mainly these thin contact layers of matrix and the bond planes between adjacent aggregate pieces, in which the microcracking is concentrated [Fig. 1(*e*)].

In Hypothesis II, shear stiffness on an individual microplane is neglected, and the overall shear stiffness of the microplane system is obtained entirely from the normal stiffnesses on the microplanes, i.e., from changes of distance. This hypothesis has the advantage of simplicity. A more sophisticated microplane model that takes into account the shear stiffnesses and inelastic slips on individual microplanes has been developed in a parallel study (5). It is needed, however, only for triaxial compressive failures and seems too complicated for the present purpose.

Let us now outline the derivation of stiffness matrix made in Ref. 9. Equilibrium conditions may be expressed by means of the principle of virtual work:

$$\delta W^c = \frac{4}{3}\pi s_{ij}\delta e_{ij} = 2\int_S s_n \delta e_n f(\vec{n}) dS \quad \ldots\ldots (3a)$$

in which S represents the surface of a unit hemisphere; the factor $(4\pi/3)$ = the volume of a sphere of radius 1; and $dS = \sin\phi d\theta d\phi$ [Fig. 1(*f*)]. Note that the integration need not be made over the entire surface of

the sphere, since the values of s_n, as well as e_n, are equal at any two diametrically opposite points on the sphere. Function $f(\vec{n})$, introducing the relative frequency of the microplanes of various orientations, $\vec{n}$, characterizes the initial anisotropy of the material. For concrete, initial isotropy may be assumed, and then $f(\vec{n}) \equiv 1$.

Substituting Eqs. 1–2 into Eq. 3*a*, we get

$$\frac{2\pi}{3} s_{ij}\delta e_{ij} = \int_S \frac{ds_n}{de_n} n_i n_j \delta e_{ij} f(\vec{n}) dS \quad \ldots\ldots (3b)$$

and because this must hold for any δe_{ij}, we must have

$$s_{ij} = \frac{3}{2\pi}\int_0^{2\pi}\int_0^{\pi/2} \frac{ds_n}{de_n} n_i n_j f(\vec{n}) \sin\phi d\phi d\theta \quad \ldots\ldots (4)$$

Furthermore, according to Eq. 1, $ds_n = (ds_n/de_n)\, de_n = (ds_n/de_n)\, n_k n_m de_{km}$, and thus, the differentation of Eq. 4 finally yields

$$ds_{ij} = D^c_{ijkm} de_{km} \quad \ldots\ldots (5)$$

in which $D^c_{ijkm} = \frac{3}{2\pi}\int_0^{2\pi}\int_0^{\pi/2} a_{ijkm} \frac{ds_n}{de_n} f(\vec{n}) \sin\phi d\phi d\theta,$

with $a_{ijkm} = n_i n_j n_k n_m \quad \ldots\ldots (6)$

in which D^c_{ijkm} = the tangent stiffnesses of the microplane system. Because the sequence of subscripts of D^c_{ijkm} is immaterial, there are only 6 independent values of incremental stiffnesses.

Considering elastic deformation of isotropic material, $f(\vec{n}) = 1$, one finds that the matrix in Eq. 6 always yields Poisson ratio, $\nu^c = 1/4$, and also $E^c = E_n/2$, in which E^c is the Young's modulus of the material, and E_n is the initial normal stiffness for the microplane. Since $\nu^c = 1/4$ is not quite true for concrete, a correction is needed. This adjustment can be made according to the following hypothesis.

Hypothesis III.—The total macroscopic strain, ϵ_{ij}, is a sum of strain, e_{ij}, due to the microplane system and additional elastic strain, ϵ^a_{ij}, i.e.,

$$\epsilon_{ij} = e_{ij} + \epsilon^a_{ij} \quad \ldots\ldots (7)$$

According to this hypothesis, we may write $\delta W = \sigma_{ij}\delta\epsilon_{ij} = \sigma_{ij}\delta\epsilon^a_{ij} + \sigma_{ij}\delta e_{ij}$ in which σ_{ij} = applied macroscopic stress. Summing the virtual works due to $\delta\epsilon^a_{ij}$ and δe_{ij} yields $\delta W = \sigma^a_{ij}\,\delta\epsilon^a_{ij} + s_{ij}\delta e_{ij}$, in which σ^a_{ij} = stress corresponding to ϵ^a_{ij}. Since both expressions for δW must hold for any $\delta\epsilon^a_{ij}$ and any $\delta\epsilon_{ij}$, it follows that $s_{ij} = \sigma^a_{ij} = \sigma_{ij}$. The superposition of strains according to Hypothesis III may be illustrated by the rheologic model in Fig. 1(*g*). The coupling of the additional elastic element is in series.

The compliances corresponding to the additional elastic strains, ϵ^a_{ij}, must satisfy isotropy conditions, and so

$$C^a_{ijkm} = \frac{1}{9K^a}\delta_{ij}\delta_{km} + \frac{1}{2G^a}\left(\delta_{ik}\delta_{jm} - \frac{1}{3}\delta_{ij}\delta_{km}\right) \quad \ldots\ldots (8)$$

in which δ_{ij} = Kronecker delta; K^a and G^a are certain additional bulk and shear moduli (constants), which cannot be less than the actual initial

bulk and shear moduli K and G. For fitting of direct tensile test data and fracture test data, it may be assumed that $1/G^a = 0$. Due to series coupling, we may now write the incremental stress-strain relation as

$$d\sigma_{ij} = D_{ijkm} d\epsilon_{km}, \quad \text{with} \quad [D_{ijkm}] = [(D^{c^{-1}})_{ijkm} + C^a_{ijkm}]^{-1} \quad \ldots\ldots\ldots\ldots (9)$$

Let us now determine the value of K^a needed to achieve the desired Poisson ratio, ν, under the assumption that $1/G^a = 0$. Let superscripts c and a distinguish between the values corresponding to D^c_{ijkm} and C^a_{ijkm}. For uniaxial stress, we have $\epsilon_{11} = \sigma_{11}/9K^a + \sigma_{11}/E^c$ and $\epsilon_{22} = \sigma_{11}/9K^a - \nu^c\sigma_{11}/E^c$, in which $\epsilon_{22} = -\nu\epsilon_{11}$, $\nu^c = 1/4$. Solving for K^a, we get:

$$K^a = \frac{1+\nu}{9(\nu^c - \nu)} E^c \quad (\text{for} \quad \nu \leqq \nu^c) \quad \ldots\ldots\ldots\ldots\ldots\ldots\ldots\ldots\ldots\ldots (10)$$

We may now write $\epsilon_{11} = (1/E^c)[\sigma_{11} - \nu^c(\sigma_{22} + \sigma_{33})] + (1/9K^a)(\sigma_{11} + \sigma_{22} + \sigma_{33}) = (1/E^c)[(1 + \nu^c)/(1 + \nu)][\sigma_{11} - \nu(\sigma_{22} + \sigma_{33})]$.

As a consequence, the microplane model describes the elastic behavior of a material having Young's modulus E under the condition that the Young's modulus of the microplane system is $E^c = [(1 + \nu^c)/(1 + \nu)]E$, and that the initial normal stiffness of each microplane is $E_n = 2[(1 + \nu^c)/(1 + \nu)]E$.

In the modeling of direct tensile tests and tensile fracture, compressive normal strains on any plane generally remain within the elastic range, and no significant unloading occurs after tensile strain-softening. For such behavior, it suffices to specify the stress-strain relation for the microplanes only for loading. It must describe cracking all the way to complete fracture, at which s_n reduces to zero. It is clear that s_n as a function of e_n must first rise, then reach a maximum, and then gradually decline to zero. We choose the final zero value to be attained asymptotically, for 2 reasons: (1) No precise information exists on the final strain at which $s_n = 0$; and (2) a smooth curve is convenient computationally. The following expression was used in previous fitting of direct tensile tests and fracture tests:

$$s_n = E_n e_n e^{-(e_n/\epsilon_o)^p} \quad \ldots\ldots\ldots\ldots\ldots\ldots\ldots\ldots\ldots\ldots\ldots\ldots\ldots\ldots\ldots\ldots (11)$$

in which E_n, ϵ_o, and p = positive constants. For p, any value between $p = 1$ and $p = 2$ seems acceptable. In this study, the values $p = 1$ and $\epsilon_o = 0.23 \times 10^{-3}$ have been adopted [Fig. 1(*h*)]. For e_n tending to zero, Eq. 11 becomes, in the limit, $s_n = E_n e_n$, which characterizes the elastic behavior of the material (with $\nu^c = 0.25$).

Crack Shear Modeling

For the modeling of crack shear, we now propose to treat the cracks—not only partially developed discontinuous cracks but also complete, continuous cracks—as a crack band of a certain characteristic width, w_c, which is the same as that used for the modeling of tensile fracture of concrete. Four distinct arguments can be offered for taking this approach.

1. Heterogeneity and Tortuosity: Due to the heterogeneous microstructure consisting of hard aggregate pieces embedded in a soft matrix,

the actual stresses in the microstructure exhibit a huge statistical scatter, and the stresses used in structural analysis can be interpreted only as statistical averages of the actual stresses taken over a certain representative volume. As is known from the theory of randomly heterogeneous media, the representative volume should be considered at least several times the size of the inhomogeneity, i.e., the aggregate size. It thus cannot make any significant difference whether the crack is modeled as a line, perfectly straight, or as a smeared band (4). The same conclusion follows when we consider crack roughness, i.e., the tortuosity of the crack surface. The asperities on the crack surface are again roughly of the size of aggregate, and so a band of one or a few aggregate sizes in width represents the actual crack at least as well as a straight line.

2. Prior Microcracking: Even if attention is restricted to distinct, continuous, fully formed cracks, one should realize that the crack must have been formed before. During its formation, concrete must have been microcracked over a zone wider than the aggregate size. Therefore, a band of microcracks must exist on the side of a distinct continuous crack in concrete.

3. Computational Convenience: The crack band model appears to be computationally more convenient than the line crack model in the analysis of crack propagation by finite elements. When a line crack extends through a certain node, the node must be split into two nodes. Consequently, the total number of nodes increases and the topological connectivity of the mesh is altered, which complicates programming for propagating cracks. Moreover, if the direction of crack propagation is not known in advance, the line interelement crack model requires making trial calculations for various possible locations of the node ahead of the crack front through which the crack should pass. The smeared cracking approach, introduced by Rashid (31), avoids these difficulties. The cracking is modeled simply by adjusting the elastic stiffnesses, and no additional nodes need be introduced. Cracks of arbitrary direction can be modeled with a fixed mesh, approximating them as a zig-zag crack band (6).

4. Numerical Equivalence: It has been demonstrated for tensile fracture, with both sudden stress drop and gradual strain-softening, that the predictions of failure loads in fracture tests are about the same for the sharp interelement crack and crack band models, provided the mesh is not too crude (10).

How can the crack band model simulate the resistance to shear, and in particular, the opening induced by shearing of the crack (dilatancy)? We can illustrate it with the help of Figs. 1(*b–d*). Imagine starting with an intact concrete block. A horizontal crack, modeled as a band [Fig. 1(*b*)], is produced by uniaxial tensile stress σ, in the vertical direction, which is simulated numerically by incrementing strain ϵ through the strain-softening range until σ becomes almost zero. Subsequently, either a shear stress τ or a shear strain γ, depending on the conditions of the simulated stress, is gradually applied in small increments. Doing this, the normal strain on the microplanes inclined +45° is increased [Fig. 1(*c*), right], and so s_n remains close to zero on these microplanes. However, e_n on the microplanes inclined −45° is decreased [Fig. 1(*c*), left], and so contrac-

tion (unloading) occurs on those microplanes. For contraction, the normal stiffness is nonzero and large.

Therefore, the shearing produces in the crack band a set of inclined compression forces shown in Fig. 1(*d*). These inclined forces have a component along the crack, which may be regarded as the crack friction, and a component normal to the crack, representing the pressure opposing dilatancy. If such a pressure is not resisted by the support conditions, then a simultaneous expansion (dilatancy) occurs so as to reduce the normal force component to zero.

In the case of a continuous rough crack, the microplanes may be imagined to mainly correspond to the planes of contact between aggregate pieces, which have various inclinations with regard to the overall crack plane. The increase in the number of inclined contacts caused by shear slip corresponds to the stiffening due to unloading normal fraction of the microplanes of −45° inclination, and the loss of contact for other contact plane inclinations corresponds to further normal extension on the microplanes of +45° inclination. It should be noted that there are always many microcracks near a continuous crack, and the microplanes also model these microcracks.

In contrast to the modeling of tensile fracture, the modeling of shear obviously requires a realistic stress-strain relationship [Figs. 1(*j–k*)] for unloading on the microplanes. The choice of this relationship is an empirical matter, and after numerical experimentation with many types of functions, the following stress-strain relations for the microplanes have been found acceptable.

Inelastic Loading in Compression.—The stress-strain relationship for the microplane is assumed to have a horizontal plastic plateau, and the following formula, with $2/\pi$ as a convenience factor, is introduced:

$$s_n = \frac{2}{\pi}|\sigma_o| \arctan(\omega e_n) \quad \text{with} \quad \omega = \frac{\pi E_n}{2|\sigma_o|}, \quad E_n = 2E\frac{(1+\nu^c)}{(1+\nu)} \qquad \text{(12)}$$

in which σ_o = the asymptotic plastic stress value. A typical curve given by Eq. 12 is plotted in Fig. 1(*i*). Numerical trials have shown that the overall compressive tensile strain-softening can be modeled, even if no strain-softening is assumed for compression on the individual microplanes.

Unloading in Tension.—Since no direct observations of unloading contraction after tensile strain-softening seem to exist, the formulas must be based on speculation, although a check is possible by comparisons with test data for crack shear. At the onset of unloading, the tangential stiffness should obviously be quite low and should further gradually increase as the cracks are getting compressed. As the compression strength is approached, the tangential stiffness should again decrease. The limiting compressive stress should be of the same order of magnitude but somewhat smaller than the compressive strength for monotonic loading, because the previous strain-softening must have caused some strength and stiffness degradation. For decreasing tensile preload, the subsequent compression response should gradually approach that for monotonic compression. Based on these considerations, the following formula for the unloading after tension appears suitable:

$$s_n = -a + \beta \arctan\left[\frac{E_n'}{\beta}(e_n - b)\right], \quad \text{with} \quad a = -\left(\sigma_\infty + \frac{\beta\pi}{2}\right),$$

$$b = \epsilon^* - \frac{\beta}{E_n'}\tan\frac{\sigma^* + a}{\beta} \qquad \text{(13)}$$

in which E_n', β and σ_∞ are 3 additional material constants that define the unloading response; and ϵ^*, σ^* are the coordinates of the reversal point at which unloading begins. A typical form of Eq. 13 is plotted in Figs. 1(*j–k*).

Parameters σ_∞, E_n' and β must depend on the previously reached maximum strain ϵ^* (reversal point). The assumed dependencies are plotted in Figs. 1(*l–n*). These curves may be characterized by the following formulas:

$$\frac{\sigma_\infty}{f_c'} = a'\frac{b' + c'\epsilon^{*n'}}{1 + c'\epsilon^{*n'}}, \quad \frac{E_n'}{E_n} = a''\left[1 + b''e^{-c''\epsilon^{*n''}}\right], \quad \frac{\beta\pi}{\sigma_\infty} = \frac{a''' + b'''\epsilon^{*2}}{1 + b'''\epsilon^{*2}} \qquad \text{(14)}$$

in which $a' = 0.58$; $b' = 1.86$; $c' = 15 \times 10^5$; $n' = 3$; $a'' = 0.07\,(f_c'/31.5)^2$; $b'' = (31.5/f_c')^2\,[14.3 - (f_c'/31.5)^2]$; $c'' = 14$; $n'' = 0.25$; $a''' = 2$; $b''' = 146{,}000$.

Reloading.—For monotonic shear loading of cracks, unloading in compression and reloading in tension do not seem very important. They would be, however, important for reversed shear and cyclic shear loading of cracks. One may speculate that the reloading curve for the microplanes would have the shape sketched in Fig. 1(*k*), which could be described by a formula of the type:

$$s_n = \sigma^{**}\exp\frac{E_n''}{\sigma^{**}}(e_n - \epsilon^{**}) \qquad \text{(15)}$$

in which ϵ^{**} and σ^{**} defines the point at which the reloading begins [Fig. 1(*k*)], and E_n'' characterizes the initial stiffness for reloading, which depends on ϵ^{**}. The last equation could not be checked, however, against any test data.

Computational Aspects

The integral in Eq. 6 has to be evaluated numerically. It may be approximated by a finite sum (8,9)

$$D_{ijkm}^c = \sum_{\alpha=1}^{N} w_\alpha \left[a_{ijkm}\frac{ds_n}{de_n}\right]_\alpha \qquad \text{(16)}$$

in which subscripts, α, refer to the values at certain numerical integration points on a unit hemisphere (i.e., certain directions); and w_α are the weights associated with the integration points. Since, in finite element programs for incremental loading, the numerical integration needs to be carried out a great number of times, a very efficient numerical integration formula is needed. For the slip theory of plasticity, the integration was performed using a rectangular grid in the θ-ϕ plane. This

approach is, however, computationally inefficient, because the integration points are crowded near the poles and, in the θ-ϕ plane, the singularity arising from the poles takes away the benefit from the use of a high-order integration formula.

Optimally, the integration points should be distributed over the spherical surface as uniformly as possible. A perfectly uniform subdivision is obtained when the microplanes normal to the α-directions are the faces of a regular polyhedron. A regular polyhedron with the most faces is the icosahedron, for which $N = 10$ (1/2 the number of sides); such a formula was proposed by Albrecht and Collatz (1). Numerical experience revealed, however, that 10 points are not enough when strain-softening takes place. The reason is that the strain-softening curves that are obtained for uniaxial tensile stresses oriented at various angles with regard to the α-directions significantly differ from each other, even though within the strain-hardening range, the differences among these curves are small (9,11). Therefore, more than 10 points are needed, and then a perfectly uniform spacing of α-directions is impossible.

Various numerical integration formulas with more than 10 integration points are given in the book by Stroud (34). All calculations in this study are based on McLaren's formula (25,34) which has 25 points per hemisphere, is symmetric with regard to the Cartesian coordinate planes, and is of degree 11 (i.e., integrates exactly all polynomials up to the 11th degree). For plane stress states, only 16 points need actually be used for the 25-point formula, because of orthogonal symmetry. Further optimum integration formulas are derived in Ref. 8 on the basis of Taylor series expansions; they involve 16, 21, 33, 37, and 61 points per hemisphere and are of degrees 9 to 13. The 61 point, 13th degree formula is highly accurate (8), more than necessary for the present purposes. For crude calculations, the 16-point or 21-point formulas of degree 9 might suffice (8).

The following numerical algorithm (9) may be used for the microplane model:

1. Determine $e_n^{(\alpha)}$ from Eq. 1 for all directions $\alpha = 1, \ldots, N$. In the first iteration of the loading step, use ϵ_{ij} for the end of the previous step and, in subsequent iterations, use the value of ϵ_{ij} determined for the mid-step in the previous iteration. In structural analysis, repeat this for all finite elements and for all integration points within each element.
2. For all directions $n^{(\alpha)}$, evaluate ds_n/de_n for use in Eq. 16. Also check for each direction whether unloading occurs, as indicated by violation of the condition $s_n \Delta e_n \geqq 0$. If violated, use for ds_n/de_n the unloading curve.
3. Evaluate D^c_{ijkm} from Eq. 6 and D_{ijkm} from Eq. 9. In structural analysis, repeat this for all elements and all integration points in each element. When solving just the stress-strain curves, as we do here, calculate then the increments of unknown stresses and unknown strains from Eq. 9. When analyzing a structure, solve (by the finite element method) the increments of nodal displacement from the given load increments, and subsequently calculate the increments of ϵ_{ij} and σ_{ij} for all elements and all integration points in each element. Then advance to the next iteration of the same loading step, or to the next loading step.

Comparison with Experimental Data

A computer program has been written for calculating the response of a crack band to imposed normal and tangential relative displacement histories or applied strain histories. The displacements reported in tests have been considered to occur over the width of the crack band, for which various values have been used in calculations, typically $0.5d_a$, d_a, and $2d_a$, in which d_a is the maximum aggregate size [Fig. 2(*a*)]. In almost all cases, the crack band width has been considered equal to d_a. The program begins by simulating the formation of the crack. To this end, normal displacement in the x-direction [Fig. 5(*a*)] is incremented until the crack opening ($\delta_n = w_c \epsilon_x$) reaches the initial value specified in the tests. Subsequently, both normal and shear displacements (or strains) are applied in small increments, the response in each loading step is solved from the incremental stiffness equations (Eq. 9) and the results are plotted and compared with test data. Since the material parameters are few, and their effect can be intuitively judged, a trial-and-error approach suffices to achieve satisfactory fits.

Paulay and Loeber's Tests (28).—These are rather extensive data, which were used in previous theoretical studies (7) and appeared to be most useful for identifying the material parameters in Eqs. 12–15. Both the

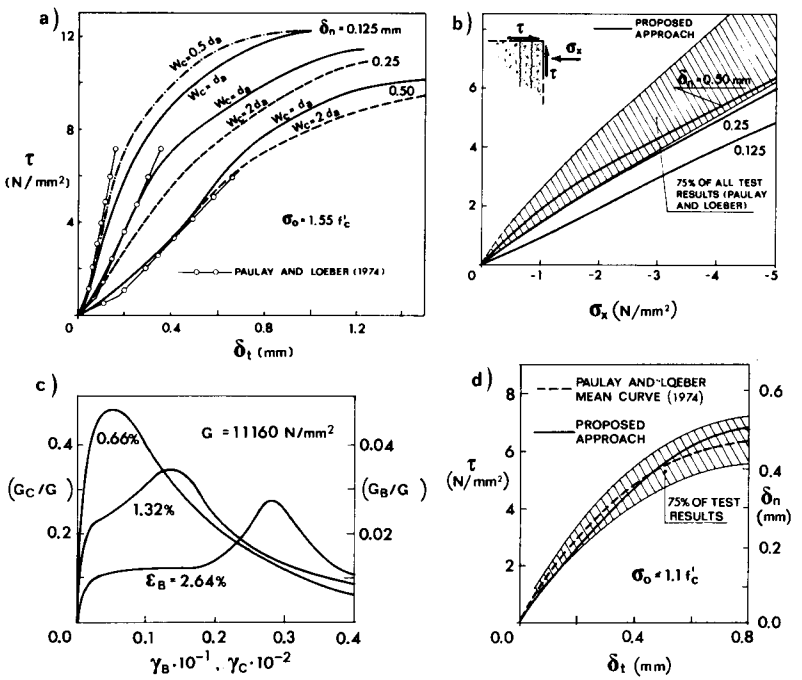

FIG. 2.—(*a–b*) Fits of Paulay and Loeber's Test Results at Constant Crack Opening; (*c*) Theoretical Curves of Shear Moduli at Constant Crack Opening (f'_c = 31.5 N/mm², d_a = 19 mm); (*d*) Fits of Paulay and Loeber's Test Results at Constant Ratio, δ_n/τ

crack slip and the opening displacement were controlled in these tests. The aggregate size was d_a = 19 mm. The response was measured for 3 different values of the crack opening displacement δ_n (0.125, 0.25 and 0.5 mm). The optimum fits achieved are shown in Fig. 2(*a*). The response curves are calculated for various values of the assumed crack band width w_c. However, for the model to be objective, one and the same value of the crack band width must of course be considered for all computations. The best compromise is approximately $w_c = d_a$. This is less than the value previously used to fit fracture test data (10), which was $w_c = 3d_a$. This value was needed to fit closely both the fracture tests and the direct tensile tests. The corresponding histories of normal stress, σ_x, produced by shearing are plotted in Fig. 2(*b*) against the shear stress, τ. The calculated responses yield somewhat larger confining normal stresses than the test data shown. This might be due to the neglect of shear stiffness on the microplanes in the present version of the model (this stiffness could, of course, be included, see Ref. 5, but the theory would become more complicated).

In Fig. 2(*c*), the tangent shear modulus, G_B, of the calculated crack band response is plotted as a function of the mean shear strain, γ_B, of the crack band, for different values of the mean tensile strain $\epsilon_x = \delta_n/w_c$. The results are shown in terms of the ratio to the shear modulus, G, of intact concrete. The stiffness decreases with increasing crack opening, as expected.

In practical situations, concrete would often be intersected by a system of parallel crack bands of a certain spacing, s. The overall deformation is then a sum of the deformations of the crack bands and of the intact concrete between the bands, both being subjected to the same shear stress. Thus, the overall averaged shear modulus, G_c, of the concrete intersected by parallel crack bands appears to be much higher than that for the crack band alone, and is much closer to the shear modulus of the intact concrete: roughly, $G_c = G_B s/w_c$. For ϵ_B = 0.66% [Fig. 2(*c*)] and for s = 190 mm, the value of G_c can be as high as $0.5G$ [$G = E/2(1 + \nu)$ = 11,159 N/mm^2 for ν = 0.18 and f'_c = 31.5 N/mm^2].

Paulay and Loeber also made tests in which the crack opening δ_n was forced to be proportional to the shear stress τ. Fig. 2(*d*) shows such test data and the theoretical response for $\delta_n = 0.074\tau$ (τ in N/mm^2, δ_n in mm). One can see a good agreement of the present theory with measurements. As pointed out by Paulay and Loeber, tests at increasing crack opening produce a greater interface damage than the tests at constant crack opening, and for this reason they generally exhibit a softer response. In Eqs. 12, 13, and 15, the material constants have been optimized with regard to the fitting of the tests at variable crack opening, rather than at constant crack opening. For instance, the best fits of the curves at constant crack opening [Fig. 2(*a*)] were obtained with $\sigma_o = 1.55 f'_c$. Nevertheless, the value $1.10f'_c$, which transpired from the fitting of the other curves examined here, is still acceptable because the value of σ_o basically affects only the plateaus of the theoretical curves, and how large is σ_o (at different crack openings) is still open to speculation.

Walraven and Reinhardt's Tests (36).—Blocks split in two parts [Fig. 3(*a*)] by a tensile crack and fastened together by 4 external steel bars were used, and the histories of shear stress, τ, crack opening displacement, δ_n, and the confining normal stress, σ_x, as a function of the tangential displacement, δ_t, were measured. The aggregate size was d_a = 16 mm. Seven specimens were tested; for the same initial crack opening and for the same crack opening history (δ_n as a function of δ_t), the experimental response curves have been replaced by mean curves in order to make possible a comparison with the theoretical prediction. Six tests are considered here. One other test was deleted because its response curve of τ versus δ_t was strikingly softer than for the other tests. The theoretical fits achieved are shown by solid lines in Fig. 3. The agreement with test data is quite good for the shear stress response, but is less satisfactory for the confining stress. (One might wonder whether

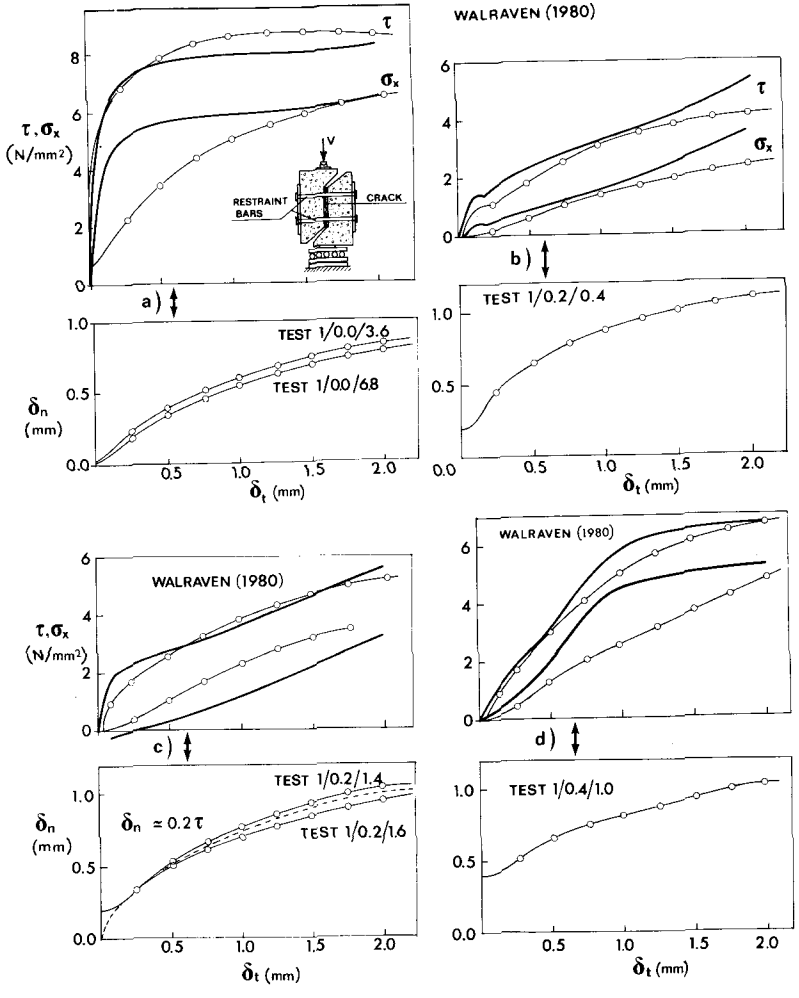

FIG. 3.—Fits of Walraven and Reinhardt's Test Results (f'_c = 31 N/mm^2, d_a = 16 mm)

this could have been caused by some initial slack in the installation of the external reinforcing bars in these tests.)

Fig. 3(*a*) compares the test data and the theoretical results for two tests with no initial crack opening. Although characterized by different restraining bars, these two tests show very similar displacements histories, and the mean history was used to obtain the theoretical prediction. Fig. 3(*c*) shows a good overall agreement for the case in which the crack opening is practically proportional to the applied shear.

Fig. 3(*b*) shows another case with a relatively large initial crack opening, $\delta_n = 0.2$ mm. For this case, the calculated curves seem to be somewhat stiff at large δ_t. Fig. 3(*d*) shows a case for a large initial crack opening, $\delta_n = 0.4$ mm. Here, the agreement of the shear stress response is very good, while the calculated confinement stress is too high for medium δ_t. Overall, if one considers that the scatter in these types of tests is quite large (standard deviation of at least 10% of the mean), the overall agreement between theory and experiment appears to be quite acceptable.

Laible, White and Gergely's Tests (23).—In these tests, precracked specimens with external restraining steel bars were used, and the shear loading was cyclic. The maximum aggregate size was 38 mm, and the initial crack opening was 0.76 mm for most tests. Numerical simulations were limited only to the first, monotonically increasing part of the first cycle. Figs. 4(*a–b*) show not only the mean measured responses (dashed lines B and E), but also the responses for the stiffest and the weakest specimens (dashed lines A, C and D, F). The displacement history is shown in Fig. 4(*c*) for Test A1. In the other tests, the path was similar. The calculated response for shear [Fig. 4(*a*), Test A1] is quite close to the mean of measured responses, while the calculated response of confining normal stress [Fig. 4(*b*)] is near the weakest experimental response. The average friction coefficient is close to 2 for the theoretical results, and close to 3.25 for the experiments. This last value seems, however, to be very high compared to other tests. In contrast to Paulay and Loeber's tests, concrete of a lower strength ($f'_c = 20.5$ N/mm^2) was used. As a consequence, the shear response of the cracks is markedly softer here. This difference seems to be correctly modeled by the previous formulas for E'_n/E_n.

Mattock's Tests (24).—Since reinforcement embedded in concrete and crossing the crack was used, evaluation is hampered by the additional uncertainty in determining the effect of dowel action. Therefore, these data are harder to evaluate theoretically. Tests MM1, MM2, and MM3, with two closed stirrups intersecting a single preformed crack at right angles (diam 9.4 mm, steel ratio 0.89%) were considered. The initial crack openings were 0.225, 0.400, and 0.625 mm, respectively. The contribution of the dowel action to the transmission of shear is estimated to be no more than 15% in Test MM1, 10% in Test MM2, while in Test MM3, this contribution is probably negligible due to early yielding of steel caused by a large initial crack opening. Thus, the effect of dowel action is probably small, due to the relatively small steel ratio and the small diameter of the stirrups.

Mattock's data are plotted in Figs. 4(*d–j*). The dowel action contribution was estimated by extrapolating the test results of Paulay, Park

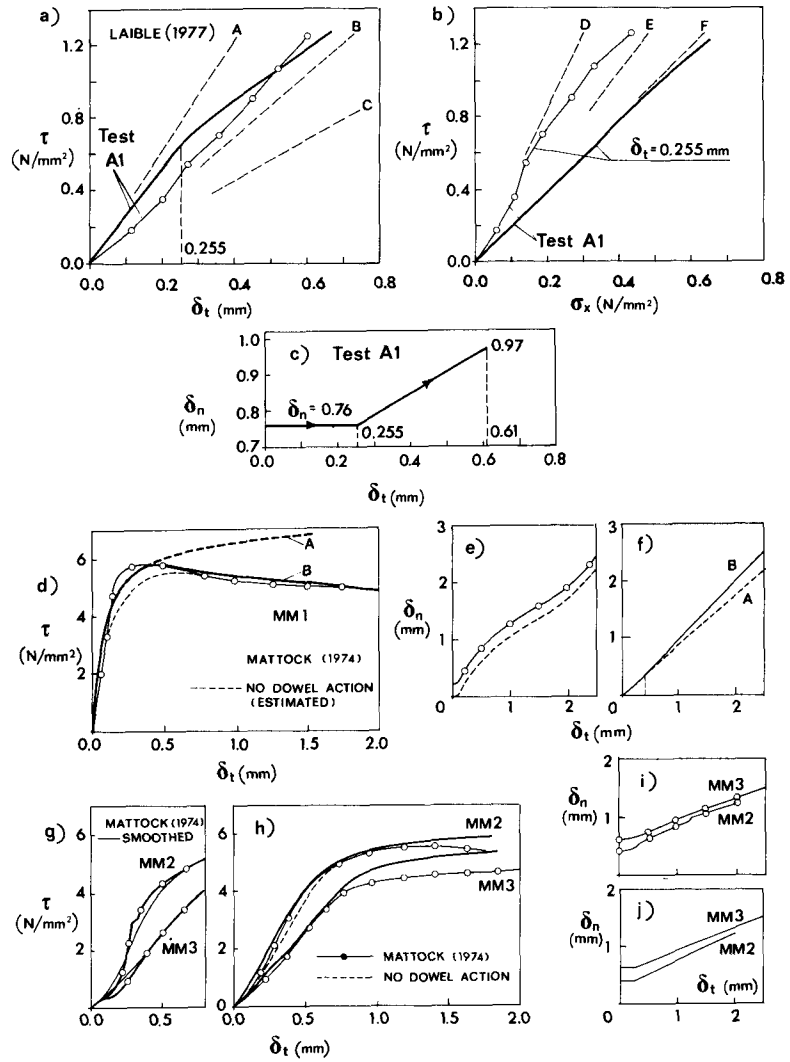

FIG. 4.—(*a–c*) Fits of Laible, White, and Gergely's Test Results ($f'_c = 20.5$ N/mm^2, $d_a = 38$ mm); and (*d–j*) of Mattock's Test Results ($f'_c = 28.4$ N/mm^2, $d_a = 19$ mm)

and Philips (29), and based on this the response curves for no dowel action were estimated as shown by the thin dotted curves in Figs. 4(*d, h*) (see also Ref. 15). The shear stress response for Test MM1, shown in Fig. 4(*d*), is somewhat too stiff for small values of δ_t, which is not the case for Tests MM2 and MM3. Perhaps the initial crack opening in Test MM1 might have been less than the reported value [see the dashed curve in Fig. 4(*e*)]. The theoretical prediction obtained with the displacement history B [Fig. 4(*f*)] matches the experimental curve well.

As for Tests MM2 and MM3, the theoretical prediction is very close

to the experimental results [Fig. 4(*h*)]. Both the experimental response curves [Fig. 5(*g*), heavy lines] and the experimental displacement histories [Fig. 4(*i*)] have been somewhat smoothed [Fig. 4(*j*)] to make it easier to compare the theoretical results and the test results.

General Loading Paths

The models that are formulated as an algebraic relation between the stresses and the relative displacements on the crack are independent of the loading path in which a given state has been reached. Therefore,

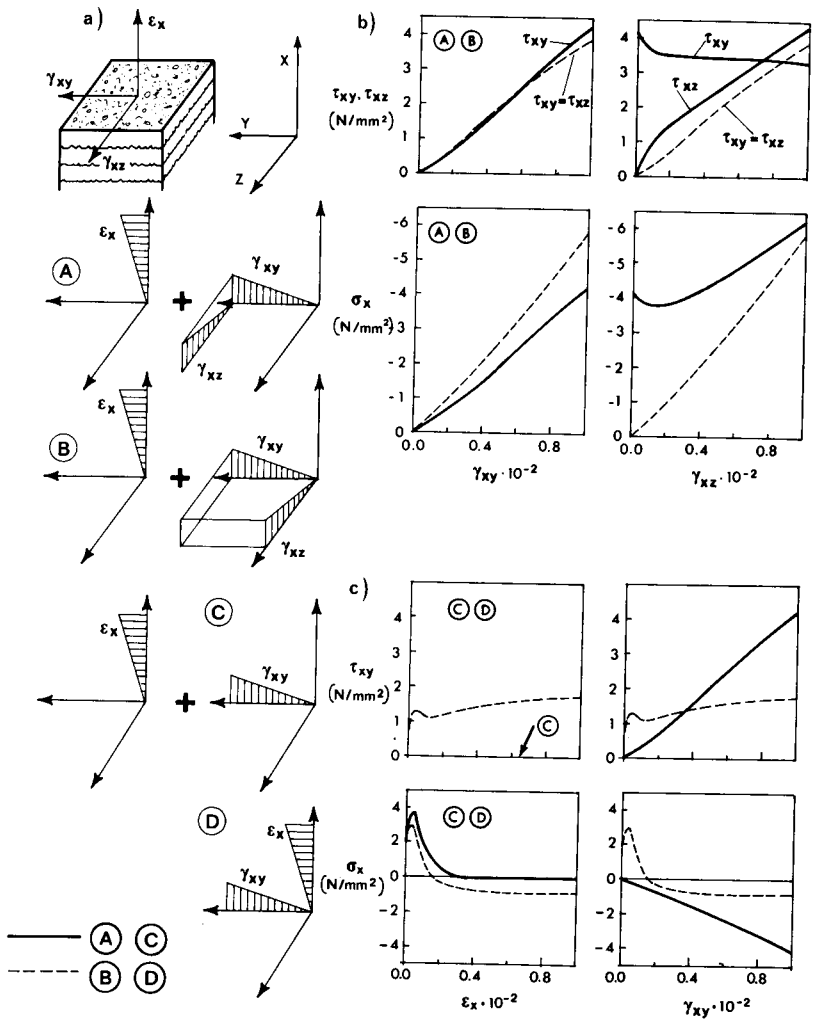

FIG. 5.—Theoretical Responses for Different Loading Paths: Conventions of Applied Strains (*a*); ϵ_x, γ_{xy}, γ_{xz} = 0–1%, $\epsilon_y = \epsilon_z = \gamma_{yz} = 0$ (*b*); ϵ_x, γ_{xy} = 0–1%, $\epsilon_y = \epsilon_z = \gamma_{yz} = \gamma_{zx} = 0$ (*c*); f'_c = 31 N/mm²

they cannot be applied to general nonproportional loading paths in which the response should significantly differ from proportional loading. The microplane model is ideally suited to describe path dependence. For different loading paths, the distribution of unloading and loading among the planes of various orientations is different, and so the overall response depends on the loading path even though the monotonic relation between stress and strain on each microplane is path-independent.

At the present, no experimental data seem to exist with regard to path-dependence of crack shear. Therefore, the present theory cannot be checked in this regard. Its application to arbitrary loadings is, however, possible since the theory is rationally based and satisfies the requirements for a general constitutive theory. Two examples are presented to illustrate the predictions for general loading paths.

The first example [Fig. 5(*b*)] compares the case when, after uniaxial cracking due to ϵ_x, either shear strains γ_{xy} and γ_{xz} are increased proportionally (Case B), or γ_{xy} is increased first, followed by an increase of γ_{xz} at constant γ_{xy} (Case A), until the same final value of shear strain is reached. As is seen from the response curves, the final states are rather different.

The second example [Fig. 5(*c*)] compares the usual case, in which concrete is first cracked by strain ϵ_x and then is loaded by shear strain γ_{xy} (Case C), with the case in which ϵ_x and γ_{xy} are increased simultaneously and proportionally (Case D), beginning from intact concrete, so that the crack is being created simultaneously with the application of shear. Again, one can see a great difference in the final states.

Conclusions

1. The crack band model, in which the relative displacements across the crack are uniformly distributed over a certain specified width of the band, is a satisfactory and computationally convenient general model for crack shear.
2. For the purpose of arbitrary general loading path, the constitutive relation of concrete within the crack band may be described by the microplane model, in which the strains on the planes of weakness of various directions within the material (the microplanes) correspond to the same macroscopic strain tensor and the stresses from all microplanes are superimposed. It appears reasonable and acceptable to neglect the shear stiffness on each microplane, so that the behavior on a microplane of any orientation may be characterized by a relation between the normal stress and strain on that microplane.
3. The crack shear response is very sensitive to the unloading law of the microplanes. Crack shearing produces contraction along the lines of a 45° inclination, in which the shearing induces large inclined compressive stresses. These stresses produce the shear stress resultant, as well as the normal confining stress across the crack, and when confinement is not provided by the support condition, crack opening due to shear results.
4. Satisfactory representation of the data from crack tests can be obtained with this model.

5. Since the same model has been previously shown capable of modeling strain-softening in the direct tensile tests, the fracture tests of notched specimens, and the deflections of cracked reinforced concrete beams, the crack band model (combined with the microplane constitutive law) appears to have a very general applicability. Thus, it should be possible to apply this model for calculating, e.g., the response to shear when the cracks are only partially formed (a system of discontinuous cracks), when the direction of shear within the microplane varies during the loading process, when the cracks are being created simultaneously with shearing, and when the material is intersected by cracks of various directions. In view of this general applicability, the model appears suitable for use in finite element programs.

Acknowledgment

Partial financial support under AFOSR Grant No. 83-0009 to Northwestern University is gratefully acknowledged. Support in the initial stage of the work was received under NSF Grant No. CEE8303148 to Northwestern University.

Appendix.—References

1. Albrecht, J., and Collatz, L., "Zur numerischen Auswertung mehrdimensionaler Integrale," *Zeitschrift für Angewandte Mathematik und Mechanik*, Band 38, Heft 1/2, Jan.–Feb., pp. 1–15.
2. Batdorf, S. B., and Budiansky, B., "A Mathematical Theory of Plasticity Based on the Concept of Slip," NACA TN1871, Apr., 1949.
3. Bažant, Z. P., "Instability, Ductility and Size Effect in Strain-softening of Concrete," *Journal of the Engineering Mechanics Division*, ASCE, Vol. 102, Paper 12042, No. EM2, Apr., 1976, pp. 331–334.
4. Bažant, Z. P., "Crack Band Model for Fracture of Geomaterials," *Fourth International Conference on Numerical Methods in Geomechanics*, Z. Eisenstein, ed., Vol. 3, University of Alberta, Edmonton, Canada, 1982, pp. 1137–1152.
5. Bažant, Z. P., "Microplane Model for Strain-Controlled Triaxial Behavior," *Mechanics of Engineering Materials*, C. S. Desai and R. H. Galagher, eds., Chapter 3, John Wiley & Sons, London, England, 1984, pp. 45–59.
6. Bažant, Z. P., and Cedolin, L., "Finite Element Modeling of Crack Band Propagation," *Journal of Structural Engineering*, ASCE, Vol. 109, No. ST1, Paper 17618, Jan., 1983, pp. 69–92.
7. Bažant, Z. P., and Gambarova, P. G., "Rough Cracks in Reinforced Concrete," *Journal of the Structural Division*, ASCE, Vol. 106, No. ST4, Paper 15330, Apr., 1980, pp. 819–842.
8. Bažant, Z. P., and Oh, B. H., "Efficient Numerical Integration on the Surface of a Sphere," *Report*, Center for Concrete and Geomaterials, Northwestern University, Evanston, Ill., 1982.
9. Bažant, Z. P., and Oh, B. H., "Model of Weak Planes for Progressive Fracture of Concrete and Rock," *Report No. 83-2/448m*, Center for Concrete and Geomaterials, Northwestern University, Evanston, Ill., Feb., 1983.
10. Bažant, Z. P., and Oh, B. H., "Crack Band Theory for Fracture of Concrete," *Materials and Structures*, (RILEM, Paris), Vol. 16, No. 94, July–Aug., 1983, pp. 155–177.
11. Bažant, Z. P., and Oh, B. H., "Microplane Model for Fracture Analysis of Concrete Structures," *Proceedings of the Symposium on the Interaction of Nonnuclear Munitions with Structures*, C. A. Ross, ed., U.S. Air Force Academy, Colorado Springs, McGregor & Werner, Inc., Washington, D.C., May, 1983.

12. Bažant, Z. P., and Oh, B. H., "Deformations of Progressively Cracking Reinforced Concrete Beams," *American Concrete Institute Journal*, Vol. 81, 1984, pp. 268–278.
13. Bažant, Z. P., and Panula, L., "Statistical Stability Effects in Concrete Failure," *Journal of the Engineering Mechanics Division*, ASCE, Vol. 104, Paper 14074, No. EM5, Oct., 1978, pp. 1195–1212.
14. Daschner, F., and Kupfer, H., "Versuche zur Schubkraftübertragung in Rissen von Normal-und Leichtbeton," *Bauingenieur 57*, 1982, pp. 57–60.
15. Eleiott, A. F., "An Experimental Investigation of Shear Transfer Across Cracks in Reinforced Concrete," thesis presented to Cornell University , at Ithaca, N.Y., in 1974, in partial fulfillment of the requirements for the degree of Master of Science.
16. Entov, V. M., and Yagust, V. I., "Experimental Investigation of Laws Governing Quasi-static Development of Macrocracks in Concrete," *Mechanics of Solids* (translated from Russian), Vol. 10, No. 4, 1975, pp. 87–95.
17. Evans, R. H., and Marathe, M. S., "Microcracking and Stress-Strain Curves for Concrete in Tension," *Materials and Structures*, (Paris), No. 1, Jan.–Feb., 1968, pp. 61–64.
18. Fardis, M. N., and Buyukozturk, O., "Shear Transfer Model for Reinforced Concrete," *Journal of the Engineering Mechanics Division*, ASCE, Vol. 105, No. EM2, Paper 14507, Apr., 1979, pp. 255–276.
19. Gambarova, P. G., "On Aggregate Interlock Mechanism in Reinforced Concrete Plates with Extensive Cracking," *Final Report of the IASBE Colloquium on Advanced Mechanics of Reinforced Concrete*, Delft, The Netherlands, June, 1981, pp. 99–120.
20. Heilmann, H. G., Hilsdorf, H. H., and Finsterwalder, K., "Festigkeit und Verformung von Beton unter Zugspanungen," *Deutscher Ausschuss für Stahlbeton*, Heft 203, W. Ernst & Sohn, West Berlin, Germany, 1969.
21. Houde, J., and Mirza, M. S., "Investigation of Shear Transfer Across Cracks by Aggregate Interlock," *Research Report No. 72-06*, Département de Génie Civil, Division des Structures, Ecole Polytéchnique de Montréal, Montréal, Canada, 1972.
22. Hughes, B. P., and Chapman, G. P., "The Complete Stress-Strain Curve for Concrete in Direct Tension," *Bulletin RILEM*, No. 30, 1966, pp. 95–97.
23. Laible, J. P., White, R. N., and Gergely, P., "Experimental Investigation of Seismic Shear Transfer Across Cracks in Concrete Nuclear Containment Vessels," *Special Publication SP53*, American Concrete Institute, 1977, pp. 203–226.
24. Mattock, A. H., "The Shear Transfer Behaviour of Cracked Monolithic Concrete Subject to Cyclically Reversing Shear," *Report SM 74-4*, Department of Civil Engineering, University of Washington, Seattle, Wash., Nov., 1974.
25. McLaren, A. D., "Optimal Numerical Integration on a Sphere," *Mathematics of Computation*, Vol. 17, 1963, pp. 361–383.
26. Pande, G. N., and Sharma, K. G., "Multi-laminate Model of Clays—A Numerical Evaluation of the Influence of Rotation of the Principal Stress Axes," *Report*, Department of Civil Engineering, University College of Swansea, U.K., 1982; see also *Proceedings, Symposium on Implementation of Computer Procedures and Stress-Strain Laws in Geotechnical Engineering*, C. S. Desai and S. K. Saxena, eds., Acorn Press, Durham, N.C., Aug., 1981, pp. 575–590.
27. Pande, G. N., and Xiong, W., "An Improved Multi-laminate Model of Jointed Rock Masses," *Proceedings, International Symposium on Numerical Models in Geomechanics*, R. Dungar, G. N. Pande, and G. A. Studer, eds., Balkema, Rotterdam, The Netherlands, 1982, pp. 218–226.
28. Paulay, T., and Loeber, P. J., "Shear Transfer by Aggregate Interlock," *Special Publication SP42*, American Concrete Institute, 1974, pp. 1–15.
29. Paulay, T., Park, R., and Phillips, M. H., "Horizontal Construction Joints in Cast-in-Place Reinforced Concrete," *Special Publication SP42*, American Concrete Institute, 1974, pp. 599–616.

30. Petersson, P. E., "Fracture Energy of Concrete: Method of Determination," *Cement and Concrete Research*, Vol. 10, 1980, pp. 78–89, and "Fracture Energy of Concrete: Practical Performance and Experimental Results," *Cement and Concrete Research*, Vol. 10, 1980, pp. 91–101.
31. Rashid, Y. R., "Analysis of Prestressed Concrete Pressure Vessels," *Nuclear Engineering and Design*, Vol. 7, No. 4, Apr., 1968, pp. 334–344.
32. Reinhardt, H. W., and Walraven, J. C., "Crack in Concrete Subject to Shear," *Journal of the Structural Division*, ASCE, Vol. 108, Paper 16802, Jan., 1982, pp. 207–224.
33. Rüsch, H., and Hilsdorf, H., "Deformation Characteristics of Concrete under Axial Tension," *Voruntersuchungen*, Bericht Nr. 44, Munich, Germany, May, 1963.
34. Stroud, A. H., *Approximate Calculation of Multiple Integrals*, Prentice Hall, Englewood Cliffs, N.J., 1971, pp. 296–302.
35. Taylor, G. I., "Plastic Strain in Metals," *Journal of Inst. Metals*, Vol. 62, 1938, pp. 307–324.
36. Walraven, J. C., and Reinhardt, H. W., "Theory and Experiments on the Mechanical Behavior of Cracks in Plain and Reinforced Concrete Subjected to Shear Loading," *HERON Journal*, Vol. 26, No. 1A, Department of Civil Engineering, University of Technology, Delft, The Netherlands, 1981.
37. Wecharatana, M., and Shah, S. P., "Slow Crack Growth in Cement Composites," *Journal of the Structural Division*, ASCE, Vol. 108, Paper 17181, June, 1982, pp. 1400–1413.
38. Zienkiewicz, O. C., and Pande, G. N., "Time-Dependent Multi-laminate Model of Rocks—A Numerical Study of Deformation and Failure of Rock Masses," *International Journal of Numerical and Analytical Methods in Geomechanics*, Vol. 1, 1977, pp. 219–247.